IET Nanobiotechnology

Research Article

IET Journals
The Institution of Engineering and Technology

Polymeric pH nanosensor with extended measurement range bearing octaarginine as cell penetrating peptide

ISSN 1751-8741
Received on 17th December 2014
Revised on 4th May 2015
Accepted on 7th May 2015
doi: 10.1049/iet-nbt.2014.0070
www.ietdl.org

Peng Ke[1], Honghao Sun[1] ✉, Mingxing Liu[1], Zhengding Su[1], Kanghong Hu[1], Hongda Zhua[1], Huilin Guo[1], Hongmei Sun[1], Thomas Lars Andresen[2], Lars Folke Olsen[3]

[1]*School of Food and Pharmaceutical Engineering, Hubei Provincial Cooperative Innovation Center of Industrial Fermentation, Hubei University of Technology, 430068 Wuhan, People's Republic of China*
[2]*Department for Micro- and Nanotechnology, Technical University of Denmark, DTU Nanotech, 2800 Lyngby, Denmark*
[3]*Department of Biochemistry and Molecular Biology, University of Southern Denmark, Campusvej 55, DK-5230 Odense M, Denmark*
✉ *E-mail: honghaosuncn@gmail.com*

Abstract: A synthetic peptide octaarginine which mimics human immunodeficiency virus-1, Tat protein is used as cell penetrating moiety for new pH nanosensors which demonstrate enhanced cellular uptake and expanded measurement range from pH 3.9 to pH 7.3 by simultaneously incorporating two complemental pH-sensitive fluorophores in a same nanoparticle. The authors believe that this triple fluorescent pH sensor provides a new tool to pH measurements that can have application in cellular uptake mechanism study and new nanomedicine design.

1 Introduction

pH nanosensors for living cells were intensely studied in recent years [1–10], because intracellular pH plays a critical role in cell, enzyme, and tissue activities, including proliferation and apoptosis, multidrug resistance, ion transport, endocytosis, and muscle contraction. Unusual intracellular pH values changes are associated with abnormal cell function, growth, and division and are observed in some common disease types such as cancer and Alzheimer's [11].

In the past decades, targeted nanomedicines delivery vehicles are beginning to play important roles in the development of new therapeutics [12, 13]. Encapsulation of drugs into delivery vehicles can improve their pharmacokinetic and pharmacodynamic properties by providing benefits including a longer blood circulation time, targeted delivery, and controlled release [12, 13]. Many of the controlled release of drugs in nanocarriers are triggered by acidic environment in cellular compartments, which can either break the acid liable bonds between nanocarrier and anititumour molecules or decompose/expand the nanocarrier, such as nanogel, micelles, and liposomes [14, 15]. The pH environment of nanoparticles experienced after cell trafficking can help us understand internalisation mechanism of nanoparticles by tumour cells and can guide the design of acid liable nanomedicines as well. A pH sensor using four 9,10-disubstituted anthracenes with different proton-binding strength was reported. The anthracenes family together can measure pH change from pH 0 to 10 [16]. Using the similar strategy, recently we have developed a ratiometric pH nanosensor bearing two complemental pH sensor fluorophores and one reference fluorophore which has advantage of measure broad pH changes ranging from pH 3.9 to 7.3 [17, 18].

More and more clues indicate that the kinetics and mechanisms of nanoparticles uptake depend critically on the surface charge and functional ligands of the nanoparticles [19]. Therefore, it is reasonable to assume that nanomedicines with different targeted moieties or cell penetrating peptides (CPPs) may have different cellular trafficking pathways and uptake kinetics. In our early stage of nanosensors study, the nanosensors prepared by reverse-microemulsion using anionic surfactant dioctyl sodium sulfosuccinate (AOT) emulsifying agent, showed negative cellular uptake [1, 2]. It is found that the trace amount of residue of AOT on the nanosensors surface lead the negative charge of nanosensors. The difficulty of cellular uptake of the nanosensors evidenced that the nanoparticles surface properties were crucial to the uptake kinetics of nanoparticles. In recent years, the potential use of CPPs as cell delivery vectors is attractive, since directed cell uptake of nanomedicines remains a major challenge in anticancer drug design. CPPs such as polyarginine showing improved drug delivery have been discovered and have been used to carry various molecules, doxorubicin, small proteins, and RNA efficiently in vitro [20–28]. Peptide with chain lengths of 8–15 arginine residues showed high cell uptake, which displayed even higher cellular uptake compared with the Tat peptide itself. However, chain lengths above 15 arginine segments show less cell uptake. Octaarginine (Arg8) conjugate medicine is reported to show a ten-fold increase in cellular uptake compared with nanomedicine without Arg8 [28]. High cellular uptake Tat-mediated pH nanosensors were reported recently [4]. However, the problem for this reported sensor is that the presence of primary amine and Tat in a same sensor leads a difficulty to distinguish whether the cellular uptake is caused by amine or Tat, because both primary amine and Tat can promote the cellular uptake.

For the purpose of enhancing pH nanosensors cellular uptake and mimic the cellular trafficking pathway as the CPPs conjugated nanomedicines, herein we designed a new generation pH nanosensor using Arg8 as cell penetrating moiety, in which the excess amine of nanoparticle (NP) is capped to prevent the cellular uptake contributed from amine.

2 Experimental section

2.1 Reagents

N-(3-aminopropyl)methacrylamide hydrochloride (AAC) is from Polymer Science Inc., N,N-methylenebis(acrylamide), acrylamide, N,N,N′,N′-tetrathylmethylenediamine (TEMED), ammonium persulfate, polyoxyethylene(4)lauryl ether (Brij30), Triton X-100, 1-hexanol, N-succinimidyl-N-methylcarbamate (NMC), dioctyl sulfosuccinate (AOT), N-hydroxysuccinimidyl, rhodamine isothiocyanate, fluorescein (FS) isothiocyanate, N-gamma-maleimidobutyryl-oxysulfosuccinimide (GMBS) ester, N-succinimidyl-NMC, tetrahydrofuran, diethyl ether, cyclohexane, and hexane were purchased from Sigma–Aldrich. Oregon green

(OG) 488 isothiocyanate was received from Invitrogen. All amino acids are purchased from GL biochem.

2.2 Gel permeation chromatography

Gel permeation chromatography experiments were performed on a SHIMADZU separation module equipped with a dual wavelength light scattering detector (VISCOTECK TriSEC model 270), a SHIMADZU ultraviolet absorbance detector (SPD-M10A), and a SHIMADZU refractive index detector (model RID-10A) and with SuperdexTM peptide column (General Electric Company (GE) Health care 10/300GL). The mobile phase is phosphate-buffered saline (PBS) buffer (0.1% wt), at a flow rate of 1 ml/min. The sample concentration is 9 mg/ml with an injection volume of 100 µl. The detection wavelength length is 280 nm.

2.3 Zeta potential

Zeta potential was measured with a ZetaPALS Zeta Potential Analyser (Brookhaven Instruments Corporation) at room temperature. Each data is the average of ten times run.

2.4 Dynamic light scattering (DLS) measurements

A 1.5 ml of pH nanosensors (0.5 mg/ml) in MilliQ water was subjected to ultrasonic treatment and filtered through a 0.45 µM needle filter before measurement. The hydrodynamic radium of the nanoparticles was measured with a ZetaPALS Zeta Potential Analyser (Brookhaven Instruments Corporation) at room temperature with a fixed scattering angle of 90 °C.

2.5 Fluorescence spectra

The fluorescence spectra were measured on FL 920 spectrometer (Edinburgh Instruments). The samples are irradiated at 488 nm (OG and FS) and 543 nm (Rh) in quartz curvet at room temperature. The dwell time is 0.2 s and scanned twice for each measurement.

2.6 Nanosensors uptake procedure

Hela cells were seeded in 35 mm culture dishes with a 10 mm microwell glass bottom, in 2 ml of Dulbecco's modified Eagle's medium containing 10% foetal bovine serum for 24 h. Cells were incubated in the presence of 1 µg/ml cationic NPs or 1 µg/ml neutral NPs for 5 h at 37 °C. The cells were washed three times with ice-cold PBS supplemented with heparin (20 units/ml) to completely remove surface-bound particles. The cells were then washed once with PBS and kept in growth medium without phenol-red for observation by confocal microscopy. The images were captured by a Leica TSC SP5 confocal microscope with a 63× water-immersed objective (Leica Microsystems, Germany).

2.7 Preparation of primary amino NPs (NPs-NH_2)

Typically, 2.04 g of acrylamide, 0.51 g of methylbisacrylamide, and 0.052 g of (3-propylamine) methylacrylamine hydrochloride were dissolved in 6.15 ml of MilliQ water. A 5.7 ml of this monomer solution was added drop wise to 240 ml of oil phase (62.5 g TX-100, 153.27 g 1-hexanol are diluted to 1000 ml with cyclohexane). After stirring for 10 min the reverse-microemulsion was formed, then the reaction mixture was degassed through freeze–vacuum–thaw for at least four cycles and kept under argon atmosphere. 60 µl of 25% (w/w) ammonium persulfate solution and 40 µl of TEMED were added to initiate the polymerisation. The reaction was stirred at room temperature for 3 h. The nanoparticles were precipitated by adding 96% ethanol and 10 ml of saline (10% wt), followed by filtrating in an Amicon ultra-filtration cell (Millipore Corporation, Bedford, MA). The NPs were dispersed into MilliQ water with ultrasonic treatment and was dialysed against MilliQ water.

2.8 Conjugation of fluorophores to NPs

About 16.6 µl of FS isothiocyanate solution (1 mg/ml in dry DMSO), 19.7 µl of OG isothiocyanate solution (1 mg/ml in dry DMSO), 35 µl of rhodamine isothiocyanate solution (1 mg/ml in dry DMSO) were added to 1 ml aqueous solution containing 50 mg NPs-NH_2 followed by adding sodium bicarbonate/sodium carbonate buffer (pH 9). The reaction mixture was stirred for 4 h and dialysed against MilliQ water for 4 days to remove free fluorophores and DMSO. Fluorescence spectroscopy was used to study the conjugation efficiency of fluorophores. The pH nanosensors (NPs-OG-FS-Rh) aqueous solution were excited with wavelengths 488 nm and 543 nm, and with these excitations the fluorescence spectra showed maximal fluorescence wavelengths at 520 and 580 nm, which contributed from OG/FS and Rh, respectively. By measuring pure OG, FS, and Rh fluorescence intensities at 520 nm and 580 nm at different aqueous concentrations, fluorescence intensity/dye concentration calibration curves of pure OG, FS, and Rh can be plotted. The number of conjugated OG, FS, and Rh molecules in pH nanosensors can be determined by their fluorescence intensity/concentration calibration curves. The result indicated that the conjugation efficiency of OG, FS, and Rh to NPs is about 80%.

2.9 Preparation of HS-Arg8

The peptide was prepared by solid phase peptide synthesis using Novasyn TGR resin as solid support. For each coupling of the amino acid, 2-(7-aza-1H-benzotriazole-1-yl)-1,1,3,3-tetramethyluronium hexafluorophosphate with 2,4,6 trimethyl pyridine was used as coupling agent. De-protection of the fluorenylmethyloxycarbonyl (Fmoe) group in each step was carried out by using 20% piperidine in dimethylformamide. The final peptide was cleaved from the resin using the cleavage cocktail containing trifluoroacetic acid (TFA) and triisopropylsiline in methylene chloride. After evaporating TFA from the cleavage cocktail under vacuum, the peptide was precipitated into excess of cold diethyl ether. The peptide was further purified by preparative high-performance liquid chromatography.

2.10 Conjugation of Arg8 to NPs (NP-OG-FS-RhB-GMBS-capped-Arg8)

NP-OG-FS-RhB (2 ml, 50 mg/ml) was reacted with N-GMBS ester at pH 7.5 to give maleimide having double bond which reacts with the thiol group on HS-Arg8 for 4 h to form a stable carbon–sulphur bond through Michael addition. Excess primary amine on the NP was capped by N-succinimidyl-NMC after GMBS functionalisation.

2.11 Purification of NPs

After function group was conjugated to NPs, the NPs were dialysed against MilliQ water or PBS buffer (pH6.2) using cellulose dialysis tube (molecular weight (MW) cut-off 12,000, Sigma) for 2 days.

2.12 Image analysis

The background of every image series was determined by plotting a histogram with number of pixels per intensity level for both colours [17]. The background level was identified as the main peak at low intensities, and the top of this peak was used as a measure of the background level for each colour. This value was subtracted from all images in a series and the corresponding calibration curve. Two methods have been employed for the measurements of pH. The first method utilised the Fiji processing package based on ImageJ34 for the generation of a mask with regions-of-interest (ROI's) localising

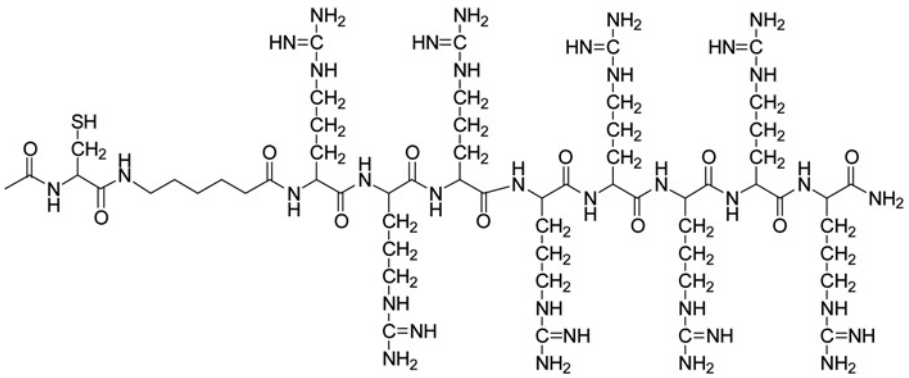

Scheme 1 *Chemical structure of HS-Arg8 used in this paper*

the nanosensor-containing vesicles. The mask was generated by addition of the two corresponding intensity images (in order to include all nanosensor-containing vesicles), the image was thresholded to produce a binary image, and all regions larger than 0.15 μm^2 were recognised as ROIs. This mask was superimposed onto the original intensity images, and mean intensity for each ROI for each colour was calculated. After background subtraction the intensity ratio of each ROI was converted to pH via the calibration curve. The second method was based on custom-made software where image preprocessing was utilised, including (i) binning of neighbouring pixels (in order to eliminate artefacts caused by sensor diffusion in between scanning the two colour channels), (ii) detection of sensor domains by comparison of the pixel intensity (of the reference dye) to the average intensity of the neighbourhood (eliminate single pixels domains), and (iii) removal of pixels with reference dye intensity lower than a cut-off. The intensities of the included pixels were converted to pH via the calibration curve. pH histograms obtained from both methods.

3 Results and discussion

The Arg8 (Scheme 1) was prepared in our laboratory by solid phase peptide synthesis. The Matrix-Assisted Laser Desorption/Ionization Time of Flight Mass Spectrometry (MALDI-TOF) showed two peaks at 1562(Arg8 plus H^+) and 1524(Arg8 plus K^+), which indicated that the Arg8 was successfully prepared (see Scheme 1).

The polyacrylamide nanoparticles containing primary amine (NP) was prepared by reverse-microemulsion polymerisation, where three monomers acrylamide, N,N-methylenebis(acrylamide) and N-(3-aminopropyl) methacrylamide hydrochloride were copolymerised. The NP containing amine was further reacted with isothiocyanate fluorophores (OG 488 [29], FS, and rhodamine (RhB) to give NP-OG-FS-RhB. In the following step, NP-OG-FS-RhB was functionalised with N-GMBS ester at pH 8.5 to give maleimide having double bond which readily reacts with the thiol group on HS-Arg8 to form a stable carbon–sulphur bond through Michael addition (Scheme 2). Excess primary amine on the NP was capped by N-succinimidyl-NMC after GMBS functionalisation. The change of primary amine to carbamide can prevent the cellular uptake caused by positively charged amine. After the NP-OG-FS-RhB (A) (+11 mV) was treated with GMBS and NMC at pH 8.5, the NP-OG-FS-RhB-GMBS-capped (B) were negatively charged with zeta potential −27 mV (Table 1), which demonstrated that the excess amine was successfully capped. After nanoparticles were conjugated with Arg8, the reverse charge of NP-OG-FS-RhB-GMBS-capped-Arg8(C) (+7 mV) proved that positively charged Arg8 was conjugated to nanoparticles. The strong negative charge of nanoparticles B (−27 mV) is caused by the hydrolysis of maleimides to maleamic acids at high pH [30]. To increase the stability of maleimides which is favourable at low pH and at the same time to facilitate the conjugation of GMBS and NMC which is favourable at high pH, pH 7.5 is used as optimal reaction condition. The following dialysis buffer with pH 6.2 is used to prevent hydrolysis of maleimides. The particle B prepared at pH 7.5 has zeta potential −2 mv, which indicates that the hydrolysis of maleimides to maleamic acids is prohibited. The final sensor NP-OG-FS-RhB-GMBS-capped-Arg8(C) prepared at

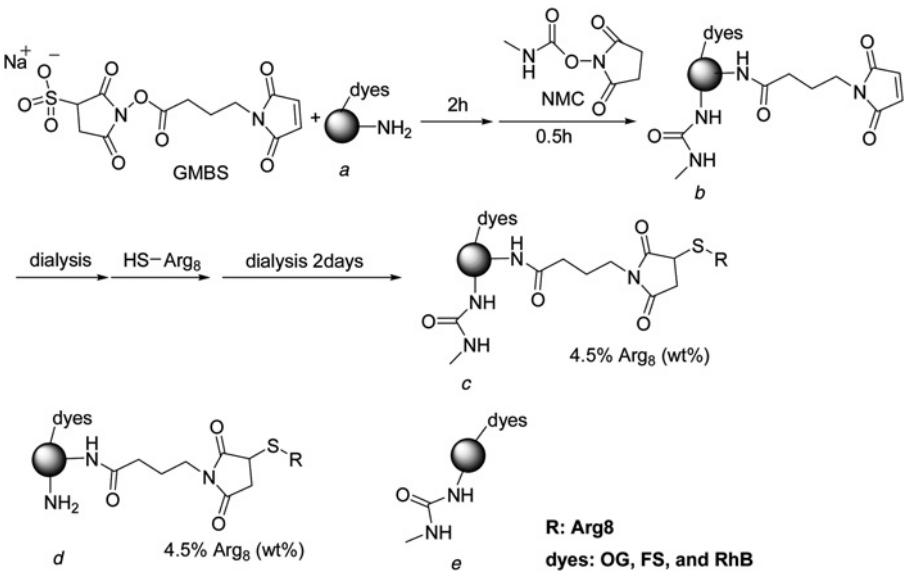

Scheme 2 *Synthetic procedure of NP-OG-FS-RhB-GMBS-capped-Arg8 and structure of NP-OG-FS-RhB-GMBS-Arg8, and NP-OG-FS-RhB-capped*

Table 1 Dynamic diameter and zeta potential (ξ) data of nanoparticles. The dynamic diameter is measured by DLS, ξ is measured by zeta potential analyser. A: NP-dye-NH2; B: NP-dye-GMBS-capped; C: NP-dye-GMBS-capped-Arg8; D: NP-dye-NH2-Arg8; E: NP-dye-capped

Name	Diameter, nm and ξ, mV
A	85 nm, +11 mV
B	75 nm, −27 mV[a]; 89 nm, −2 mV[b]
C	127 nm, +7 mV[a]; 88 nm, +11 mV[b]
D	120 nm, +12 mV[a]; 92 nm, +16 mV[b]
E	84 nm, +0.5 mV

[a]Reaction at pH 8.5, dialysis at pH 7.0.
[b]Reaction at pH 7.5, dialysis at pH 6.2.

pH 7.5 shows a positive charge +11 mv. The final nanoparticles are stable in aqueous solution, no obvious size changes are observed after 6 months.

The fluorescent spectra of NP-OG-FS-RhB-GMBS-capped-Arg8 at different pH values are shown in Fig. 1 (inset). The spectra illustrate that fluorescence intensity of OG and FS increase with pH value, whereas that of RhB keep relative constant. The calibration curve with ratio of fluorescence intensity $R = (\mathrm{OG} + \mathrm{FS})/\mathrm{RhB}$ vs. pH values are showed in Fig. 1. According to the R vs. pH calibration curve (Fig. 1), pH value can be easily read out at a given R value. The calibration curve R vs. pH can be fitted by following equation [16]

$$R = \frac{R_1}{10^{\mathrm{pKa}_1 - \mathrm{pH} + 1}} + \frac{R_2}{10^{\mathrm{pKa}_2 - \mathrm{pH} + 1}} + R_0$$

In the equation, R is the ratio of emission intensities excited at 488 and 543 nm, $R_0 = R_{\min}$ (the ratio for the fully protonated form), $(R_0 + R_1 + R_2) = R_{\max}$ (the ratio for the fully deprotonated form), and pKa is the specific pKa value for the fluorophore when incorporated into the particle. pKa_1 and pKa_2 are the specific pKa values of the two pH-sensitive fluorophores when incorporated into this particle, here OG and FS. The new pH nanosensor NP-OG-FS-RhB-GMBS-capped-Arg8 has large dynamic measurement range from pH 3.9 to pH 7.3 (Fig. 2), which can cover pH values of most physiological environment.

The final nanoparticle NP-OG-FS-RhB-GMBS-capped-Arg8 was investigated by atomic force microscopy (AFM) (Fig. 2*a*) and DLS (Fig. 2*b*). DLS indicates that the NP has diameter about 88 nm. AFM demonstrates that the NP is relative uniform.

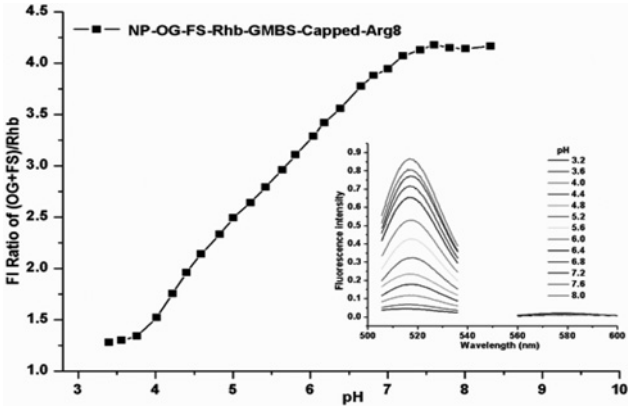

Fig. 1 *pH calibration curves of NP-OG-FS-RhB-GMBS-capped-Arg8. The fluorescence intensity ratios between pH-sensitive fluorophores OG, FS at 518 nm and reference fluorophore RhB at 578 nm were plotted against pH values. (inset) Fluorescence emission spectra of NP-OG-FS-RhB-GMBS-capped-Arg8 at different pH values. OG and FS were excited at 488 nm; RhB was excited at 545 nm*

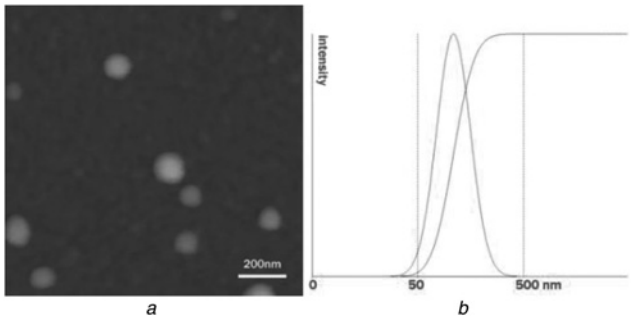

Fig. 2 *Size of nanoparticles NP-OG-FS-RhB-GMBS-capped-Arg8 was characterised by*

a AFM
b DLS

To determine whether the Arg8 coating can enhance cellular uptake properties of the nanosensors, sensors with Arg8 (NP-OG-FS-RhB-GMBS-capped-Arg8) and neutral sensors without Arg8 (NP-OG-FS-RhB-capped) (see Scheme 2) were investigated uptake in Hela cells. The cells were treated with 10

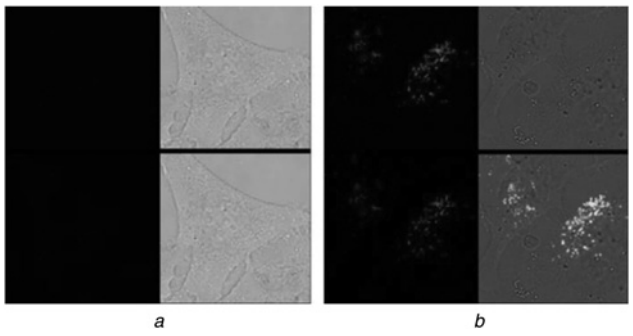

Fig. 3 *Representative confocal microscopic image of Hela cells incubated with*

a Neutral pH nanosensor NP-OG-FS-RhB-capped, in which the excess amine was capped
b pH nanosensor NP-OG-FS-RhB-GMBS-capped-Arg8. The cells were treated with 10 µg/ml of particles in medium for 3 h, then washed and visualised by a 63× water-immersed objective. Top left: OG and FS (green), top right: differential interference contrast microscope (DIC), bottom left: RhB (red) and bottom right: overlay

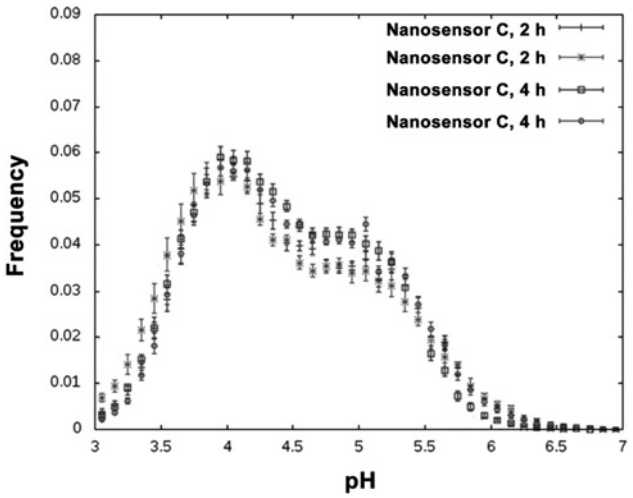

Fig. 4 *Histogram showing pH distribution of the nanosensor-containing vesicles analysed pH measurement in Hela cells at different time, nanosensor C at 2 and 4 h. Each measurement was repeated three times*

μg/ml of both neutral (NP-OG-FS-RhB-capped) and Arg8 conjugated particles (NP-OG-FS-RhB-GMBS-capped-Arg8) in serum-free medium for 3 h. After removing the non-internalised nanoparticles by washing with PBS, fluorescence images of cells were captured with a 63× water-immersed objective. As seen in Fig. 3*b*, the Arg8 conjugated nanoparticles can be taken up by cells within 3 h. In comparison, neutral nanoparticles are not taken up within 3 h, which are difficult to visualise using fluorescence microscopy (Fig. 3*a*). The cell uptake experiments show that conjugating a CPP (Arg8) introduces enhanced cellular uptake property into this type of nanoparticle.

To evaluate whether this sensor (nanosensor C) is a reliable tool to use in a cellular environment, the pH in Hela cells was measured at different time for three times. Fig. 4 showed histogram pH distribution of the nanosensor-containing vesicles in *Hela* cells at different time. The results indicate that after 2 and 4 h the pH values have two distributions at pH 4 and pH 5.2. It demonstrated that the nanoparticles were located in endosomes (pH5–6) and lysosomes (pH 4–5) compartment, which was conformed previously with the published results [18]. It is proved that this sensor can measure pH in cells.

4 Conclusions

The triple fluorophores labelled pH sensors bearing pH insensitive fluorophores (RhB) as reference and two pH-sensitive fluorophores (OG and FS) with complemental pKa were produced. The sensor was further functionalised with Arg8 and demonstrated enhanced cellular uptake compared with pH sensor without Arg8. The new Arg8 conjugated pH nanosensor has the following three advantages: extended measurement range pH 3.9–7.3; enhanced cellular uptake; and closely representing the real pH environments as polyarginine conjugated medicines experienced after cellular internalisation. We believe that this triple fluorescent pH sensor bearing CPP (Arg8) provides a new tool to pH measurements that can have application in cellular uptake mechanism study and new nanomedicine design.

5 Acknowledgments

The authors thank Kræftens Bekæmpelse and the Danish Research Council for Technology and Production (grant 274-07-0172), The Natural Science Foundation of China (51371079) Hubei Province Natural Science Fund Project (2014CFA080, 2014CFB595), Chutian Scholars Fund Project from the Education Department of Hubei Province, and Hundred Talents Program from the Organization Department of Hubei Province for financial support.

6 References

1 Sun, H.H., Scharff-Poulsen, A.M., Gu, H., Almdal, K.: 'Synthesis and characterization of ratiometric, pH sensing nanoparticles with covalently attached fluorescent dyes', *Chem. Mater.*, 2006, **18**, pp. 3381–3385
2 Sun, H.H., Andresen, T.L., Benjaminsen, R.V., Almdal, K.: 'Polymeric nanosensors for measuring the full dynamic pH range of endosomes and lysosomes in mammalian cells', *J. Biomed. Nanotechnol.*, 2009, **5**, pp. 1–7
3 Buck, S.M., Xu, H., Brasuel, M., Philbert, M.A., Kopelman, R.: 'Nanoscale probes encapsulated by biologically localized embedding (PEBBLEs) for ion sensing and imaging in live cells', *Talanta*, 2004, **63**, pp. 41–59
4 Coupland, P.G., Briddon, S.J., Aylott, J.W.: 'Using fluorescent pH-sensitive nanosensors to report their intracellular location after Tat-mediated delivery', *Integr. Biol.*, 2009, **1**, pp. 318–323
5 Chauhan, V.M., Burnett, G.R., Aylott, J.W.: 'Dual-fluorophore ratiometric pH nanosensor with tuneable pKa and extended dynamic range', *Analyst*, 2011, **136**, (9), pp. 1799–1801
6 Kumar, E.K., Pramod, L.N.F., Almdal, K., Andresen, T.L.: 'Synthesis and characterization of a micelle-based pH nanosensor with an unprecedented broad measurement range', *Chem. Mater.*, 2013, **25**, pp. 1496–1501
7 Ruedas-Rama, M.J., Orte, A., Hall, E.A.H., Alvarez-Pez, J.M., Talavera, E.M.: 'Quantum dot photoluminescence lifetime-based pH nanosensor', *Chem. Commun.*, 2011, **47**, pp. 2898–2900
8 Jin, L.H., Fang, Y.X., Shang, L., *et al.*: 'Gold nanocluster-based electrochemically controlled fluorescence switch surface with Prussian blue as the electrical signal receptor', *Chem. Commun.*, 2013, **49**, pp. 243–245
9 Nakata, E., Yukimachi, Y., Nazumi, Y., *et al.*: 'A novel strategy to design latent ratiometric fluorescent pH probes based on self-assembled SNARF derivatives', *RSC Adv.*, 2014, **4**, pp. 348–357
10 You, Q.H., Lee, Y.M., Chan, W.H., *et al.*: 'A colorimetric and ratiometric fluorescent pH probe based on ring opening/closing approach and its applications in monitoring cellular pH change', *RSC Adv.*, 2015, **5**, pp. 4099–4102
11 Han, J.Y., Burgess, K.: 'Fluorescent indicators for intracellular pH', *Chem. Rev.*, 2010, **110**, (5), pp. 2709–2728
12 van Vlerken, L.E., Vyas, T.K., Amiji, M.M.: 'Poly(ethylene glycol)-modified nanocarriers for tumor-targeted and intracellular delivery', *Pharm. Res.*, 2007, **24**, pp. 1405–1414
13 Ferrari, M.: 'Cancer nanotechnology: opportunities and challenges', *Nat. Rev. Cancer*, 2005, **5**, (3), pp. 161–171
14 Alani, A.W.G., Bae, Y., Rao, D.A., Kwon, G.S.: 'Polymeric micelles for the pH-dependent controlled, continuous low dose release of paclitaxel', *Biomaterials*, 2010, **31**, pp. 1765–1772
15 Tsai, H.C., Chang, W.H., Lo, C.L., *et al.*: 'Graft and diblock copolymer multifunctional micelles for cancer chemotherapy and imaging', *Biomaterials*, 2010, **31**, (8), pp. 2293–2301
16 Silva, A.P., Silva, S.S.K., Gooneseker, N.C.W., *et al.*: 'Analog parallel processing of molecular sensory information', *J. Am. Chem. Soc.*, 2007, **129**, pp. 3050–3051
17 Sun, H.H., Almdal, K., Andresen, T.L.: 'Expanding the dynamic measurement range for polymeric nanoparticle pH sensors', *Chem. Commun.*, 2011, **47**, pp. 5268–5270
18 Benjaminsen, R.V., Sun, H.H., Henriksen, J.R., Christensen, N.M., Almdal, K., Andresen, T.L.: 'Evaluating nanoparticle sensor design for intracellular pH measurements', *ACS Nano*, 2011, **5**, pp. 5864–5873
19 Lunov, O., Syrovets, T., Loos, C., *et al.*: 'Differential uptake of functionalized polystyrene nanoparticles by human macrophages and a monocytic cell line', *ACS Nano*, 2011, **5**, (3), pp. 1657–1669
20 Noh, S.M., Park, M.K., Shim, G., *et al.*: 'Pegylated poly-L-arginine derivatives of chitosan for effective delivery of siRNA', *J. Control. Release*, 2010, **145**, pp. 159–164
21 Sun, V.Z., Li, Z.B., Deming, T.J., Kamei, D.T.: 'Intracellular fates of cell penetrating block copolypeptide vesicles', *Biomacromolecules*, 2011, **12**, pp. 10–13
22 Lehto, T., Abes, R., Oskolkov, N., *et al.*: 'Delivery of nucleic acids with a stearylated (R×R) 4 peptide using a non-covalent co-incubation strategy', *J. Control. Release*, 2010, **141**, pp. 42–51
23 Izumisawa, T., Hattori, Y., Date, M., Toma, K., Maitani, Y.: 'Cell line-dependent internalization pathways determine DNA transfection efficiency of decaarginine-PEG-lipid', *Int. J. Pharmaceutics*, 2011, **404**, pp. 264–270
24 Lemeshko, V.V.: 'Potential-dependent membrane permeabilization and mitochondrial aggregation caused by anticancer polyarginine-KLA peptides', *Arch. Biochem. Biophys.*, 2010, **493**, (2), pp. 213–220
25 Koker, S.D., Naessens, T.B., Geest, G.D., *et al.*: 'Activity after pulmonary delivery antigen delivery tools with Th17 skewing biodegradable polyelectrolyte microcapsules', *J. Immunol.*, 2010, **184**, pp. 203–211
26 Futaki, S., Suzuki, T., Ohashi, W., *et al.*: 'Possible existence of common internalization mechanisms among arginine-rich peptides', *J. Biol. Chem.*, 2001, **276**, pp. 5836–5840
27 Won, Y.W., Kim, H.A., Lee, M., Kim, Y.H.: 'Reducible poly(oligo-D-arginine) for enhanced gene expression in mouse lung by intratracheal injection', *Am. Soc. Gene Cell Therapy*, 2010, **18**, pp. 734–742
28 van Rijt, S.H., Kostrhunova, H., Brabec, V., Sadler, P.J.: 'Functionalization of osmium arene anticancer complexes with (poly)arginine: effect on cellular uptake, internalization, and cytotoxicity', *Bioconjugate Chem.*, 2011, **22**, pp. 218–226
29 Haugland, R.P.: 'Handbook of Fluorescent Probes and Research Products' Molecular Probes, Oregon, (2002, 9th edn), pp. 840–841
30 Wu, C.W., Yarbrough, L.R., Wu, F.Y.H.: 'N-(1-Pyrene)maleimide: a fluorescent crosslinking reagent', *Biochemistry*, 1976, **15**, (13), pp. 2863–2868